Investigation on Mechanical and Magnetic Field Behaviors of GIB Plug-in Connector under Different Contact Conditions

Xiangyu Guan [1], Quanyu Shen [1], Minghan Zou [2], Naiqiu Shu [1], and Hui Peng [1]

[1] School of Electrical Engineering
Wuhan University, Wuhan, 430072, China
xiangyuguan1986@163.com

[2] State Grid Nanjing Power Supply Company
Nanjing, 210000, China
773740620@qq.com

Abstract ─ In order to provide an effective detection method for internal contact fault of gas insulated bus (GIB), mechanical and magnetic field behaviors of GIB plug-in connector under different assembly conditions are analyzed by finite element (FEM) method in this paper. Contact forces on individual contact spots are obtained by mechanical field analysis then simulated by imperfect contact bridge models during electromagnetic field analysis. Magnetic field distributions around GIB plug-in connector under the various contact statuses (conductor insert depth and docking angle) are studied through numerical modeling and field testing. Results show that the mechanical contact parameters (contact forces and radiuses) of individual contact fingers vary from each other under the action of holding spring deformation and conductor gravity, and the surrounding magnetic field has strong relationship with the internal mechanical contact status. The magnetic field strength distributes uniformly around the GIB plug-in connector under well assembly condition. However, the magnetic field distorts since mechanical contact status is changed by the contact degradation or contact failure.

Index Terms ─ Contact failure, finite element method, gas insulated bus, magnetic field, plug-in connector.

I. INTRODUCTION

Gas insulate bus (GIB) equipment are of interest in modern power transmission/distribution systems due to their advantages of environmental friendliness, large power transmission capacity, easy-maintenance and high operation reliability [1]. Numerous of slidable plug-in connectors are used as the main electrical loop connections of GIB for absorbing misalignments during manufactory/assembly process and mechanical/thermal stress during operation process [2]. Dynamic contact conditions exist between contact elements for slidable design [3], additional power loss and electromagnetic force will act on plug-in connector due to the current constriction effect, which makes GIB plug-in connector become one of the feeblest components of equipment. If the amount of contact degradation is beyond failure threshold, contact overheating fault may happen and internal flash over could be induced by poor contacts [4-5]. The GIB must be disintegrated since internal fault happens as gas pressure vessel (which is filled with about 0.4Mpa SF6 gas), power supply recovery cycle is considerable and really hard to avoid the greenhouse gas leaking. As a consequence, the contact degradation and overheating fault of the GIB plug-in connector are serious threatening to the safe operation of equipment and power systems.

Due to fearful damages by internal contact fault, several countermeasures such as the electrical loop resistance test [6-7], tank vibration monitoring [8-9], partial discharge [10-11] and temperature monitoring [12] have been investigated and applied to the GIB equipment. Each of mentioned methods has its merits on internal fault/overheating detection, however they are less effective for early stages of contact fault. Lower electrical loop resistance results do not necessarily reply good contacts due to only the total electric loop connection condition evaluated, and contact trouble on single connector may be hidden. It's hard to locate acceleration/temperature sensors inside metal enclosure due to the insulation/sealing design limits of gas insulated equipment, besides, the relationships between inner contact statuses and outer vibration/temperature are not clear. The internal contact has already disabled since detectable partial discharge happens, and there is always not sufficient time for early warning. Magnetic field behaviors can directly reflect early degradation stages of contact failures [13-14], and magnetic field detection method on bolt connections of GIB is studied in [15] by attaching magnetic sensors inside metal tank. However, few previous works has paid attention on the

Submitted On: August 8, 2016
Accepted On: January 28, 2017

relationship between the surrounding magnetic field and contact conditions of GIB plug-in connector.

The fact that assembly conditions of GIB plug-in connector can be changed under cyclic thermal loadings by operation current and environmental temperature has been revealed in our previous study [16]. In order to identify and evaluate the internal contact failure of GIB equipment effectively, relationships between internal contact status and magnetic field are obtained by three-dimensional finite element modeling in this paper. Physical structure of the GIB capsule is shown in Fig. 1. The main electrical bus gets through both ends of disc-type epoxy insulators which is fixed by slidable plug-in connectors. Mechanical and electrical connection between the socket and conductor plug are realized by series of concentric-arranged spring-loaded contact components. Magnetic fields strengths around plug-in connector (C1) are measured by electromagnetic probes. Assumptions about numerical model are as follows.

Electromagnetic field analysis is based on quasi-static approximation with the AC operation current.

Partial tiny component geometry characteristics could not obviously affect distributions of surrounding magnetic field. Based on this concept, several external insulation designing (champers on conductor surface) and supporting/fixing parts (terminal bolts and locating parts) are omitted to minimize computational effort.

Micro-rough features of both contact surfaces are neglected, and the mechanical contact area is assumed equal to electrical contact area with chemical stability of SF_6 insulation gas.

The mechanical contact is rather a stable physical condition comparing with surrounding electromagnetic field, and it can be hypothesized that the weak coupling relation exists between electromagnetic and mechanical fields of GIB plug-in connector.

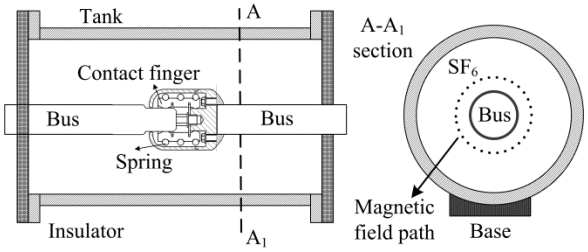

Fig. 1. Schematic structure of GIB capsule.

The research thought of this paper is organized as follows: numerical calculation method is discussed in Section II. Mechanical contact parameters (contact force and radius) of plug-in connector with various assembly conditions are calculated by mechanical FEM analysis in Section III. Electromagnetic field analysis of the GIB equipment using imperfect contact bridge model by the **A**-φ method is introduced in Section IV, and magnetic field results are given in Section V. Finally, relationship between the internal contact status and the surrounding magnetic field are summarized in Section VI.

II. NUMERICAL CALCULATION METHOD

According with the positioning design (deviation of conductor docking angle is limited) and the operation condition (thermal expansion/shrink occurred along bus line) of equipment, the contact status of GIB plug-in connector can be divided into conductor insert depth and docking angle. A sequential coupling method is adopted to analyze the mechanical and electromagnetic field behaviors under various contact conditions.

A. Mechanical contact parameters

Assembly structure of the GIB plug-in connector is described in Fig. 2 and the assembly parameters are listed on the bottom left of the figure. Conductor insert depth on the contact failure point is defined as 18 mm. Positioning design allows only radiation freedom of contact fingers along the direction of contact force, and the deviation of conductor docking angle is limited (less than 2°). Assembly conditions of plug-in connector may be changed by the cyclic thermal loading or short circuit current impact during the service life. Besides, contact forces can be reduced by service temperature, stress relaxation and time [17]. Hence, the mechanical contact statuses of the GIB plug-in connector under various assembly conditions and degradation stages should be accurately modeled for realizing the internal fault identification through magnetic field distributions.

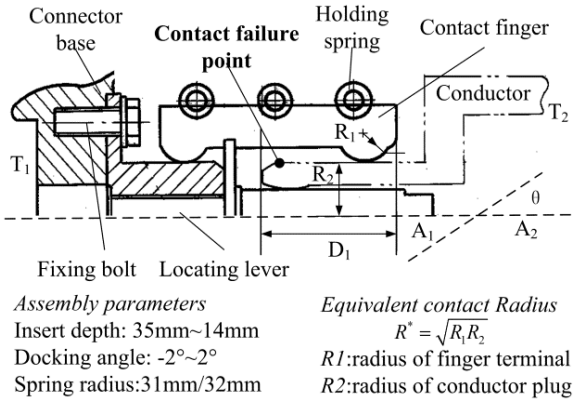

Fig. 2. Assembly structure of GIB plug-in connector.

B. Numerical calculation process

A sequential coupling method is used to analysis the magnetic field distributions around the GIB plug-in connector with various contact status and the numerical calculation flowchart is described in Fig. 3. Firstly, the contact forces of plug-in connector are calculated by mechanical field analysis. Magnetic field distributions around the GIB plug-in connector is then obtained by

electromagnetic field analysis in which the electrical contact between contact elements are simulated by the imperfect bridge model using mechanical contact forces from mechanical analysis as load inputs.

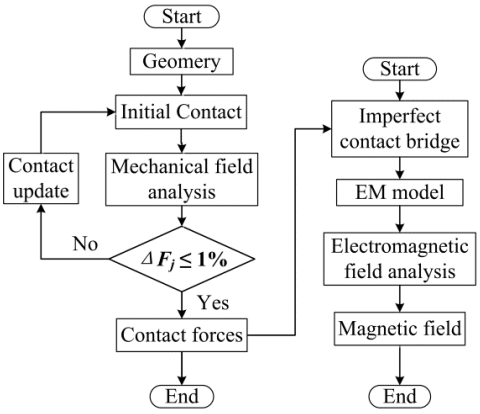

Fig. 3. Flowchart of numerical calculation.

III. MECHANICAL CONTACT ANALYSIS

The mechanical contact of GIB plug-in connector belongs to quasi-static process for the long degradation time, and forces on per contact spots are constrained by holding spring and conductor gravity.

A. Mechanical field modeling

Distribution of contact forces on individual contact fingers under action of holding spring and conductor gravity can be obtained from mechanical finite element analysis by solving displacement equation. Governing equation of static mechanical field is as follows:

$$\left.\begin{aligned}(\lambda+G)\frac{\partial e}{\partial x}+G\nabla^2 u+F_x=0\\(\lambda+G)\frac{\partial e}{\partial y}+G\nabla^2 v+F_y=0\\(\lambda+G)\frac{\partial e}{\partial z}+G\nabla^2 w+F_z=0\end{aligned}\right\}, \tag{1}$$

where λ is lame constant, G is shear modulus and E is Young's modulus, u, v, w are displacement components along space coordinate axis. F_x, F_y, F_z are extern force components along space coordinate axis.

The lame constant and the element displacement can be described as follows:

$$\lambda=\frac{E\mu_e}{(1+\mu_e)(1-2\mu_e)}, \tag{2}$$

$$e=\frac{\partial u}{\partial x}+\frac{\partial v}{\partial y}+\frac{\partial w}{\partial z}, \tag{3}$$

where μ_e means the Poisson's ratio.

Boundary conditions of mechanical field analysis are listed as follows:

$$u=v=w=0\,|_{T_1}. \tag{4}$$

Mechanical contact between contact fingers and conductor plug are analyzed using augmented Lagrange multiplier method [18]:

$$\begin{bmatrix}K+K_P & G^T\\ G & 0\end{bmatrix}\begin{bmatrix}\mathbf{r}\\ \lambda\end{bmatrix}=\begin{bmatrix}F-R\\ -g_0\end{bmatrix}, \tag{5}$$

where K is stiffness matrix of contact elements, K_p is penalty stiffness matrix between contact interfaces, G is contact potential which is defined as the product of λ and g_0, $\mathbf{r}$ is vector matrix of contact gap, λ is Lagrange multiplier, F and R are external force and reactive force (contact force) respectively.

Mechanical contact statuses of plug-in connector are in balance with the elastic deformation of holding springs and conductor gravity. Contact force acting on per contact finger is reactive force of the contact finger and the relationship between contact force and contact radius can be described by the Hertz formula [19]:

$$a=(3F_jR^*/4E^*)^{1/3}, \tag{6}$$

where a is mechanical contact radius, F_j is contact force on contact spot, R^* is equivalent radius (summarized on the bottom right of Fig. 2), E^* is equivalent Young's modulus of different contact materials:

$$\frac{1}{E^*}=\frac{1-\mu_{e1}^2}{E_1}+\frac{1-\mu_{e2}^2}{E_2}. \tag{7}$$

Mechanical stress on different contact spots under well assembly conditions (30 mm conductor insert depth) and partial loosen contact (2 degrees of docking angle deviation) are analyzed by mechanical FEM model and results are illustrated in Fig. 4. The results show that during well assembly condition, maximum mechanical stress concretes on contact spots for the limited contact area, and mechanical stresses on bottom contact fingers are larger than the upper ones under action of conductor gravity. Since the conductor docking angle deviates, the mechanical stress on the bottom contact fingers could increase up to 5.82 times higher than the one in well assembly conditions, meanwhile mechanical stress on the upper contact fingers reduced to zero, which means that mechanical contact is lost on these spots and no operation current could flow through.

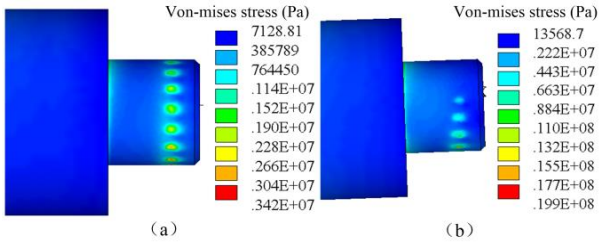

Fig. 4. Mechanical stress distributions of GIB plug-in connector under different contact conditions: (a) well assembly, and (b) conductor docking angle deviation (-2°).

Mechanical contact parameters of the GIB plug-in connector under well assembly and conductor docking angle deviation are presented in Fig. 5. Results show that the contact forces and radiuses increase from upper contact fingers to lower ones with the action of conductor gravity, and mechanical contact distributes nearly uniform among under well assembly condition. However, since the conductor docking angle deviates, mechanical contact varies obviously from each contact finger, and several bottom contact spots even lose mechanical contact (contact force reduce to 0) under seriously distorts of holding springs.

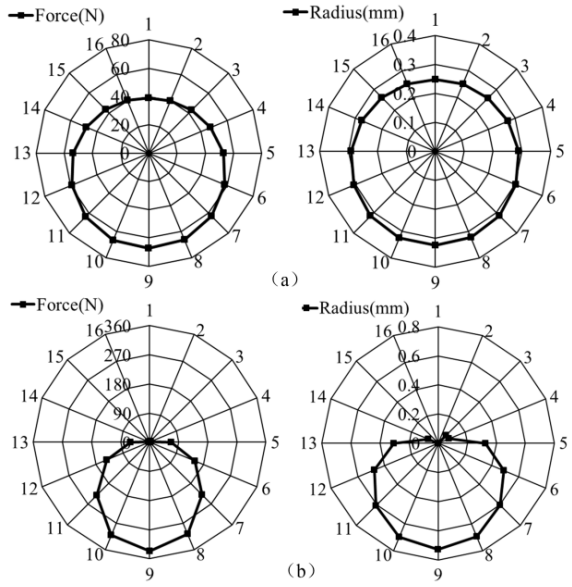

Fig. 5. Mechanical contact forces and radiuses of GIB plug-in connector: (a) well assembly, and (b) conductor docking angle deviation (-2°).

B. Electrical contact parameters

Contact resistance of plug-in connector consists only of the constriction resistance, and the relationship between resistance and contact radius is described by the Holm's contact resistance theory:

$$R_c = \rho_0 / 2a, \tag{8}$$

where ρ_0 is resistivity of contact elements and a is the equivalent radius of individual contact spot.

IV. ELECTROMAGNETIC FIELD ANALYSIS WITH POOR CONTACTS

Based on the results of mechanical contact force and radius analysis of GIB plug-in connector mentioned above, operation current flows among different contact spots can be varied from each other for deviation of the contact resistance, resulting no-uniform surrounding magnetic field distributions. A finite element model which considers the current constriction on contact spots with various mechanical contact statuses is built to obtain current and electromagnetic field behaviors of plug-in connector under different contact conditions.

A. Imperfect contact bridge model

Current conduction on contact interfaces is usually simulated by contact bridge during numerical modeling [20]. However several contact spot of plug-in connector with the poor contact status are hard to geometrically model in the electromagnetic field environment. To overcome this shortage, an imperfect contact bridge model is constructed in this paper by two parameters: the equivalent contact bridge radius and the equivalent resistivity. Mathematical expression of the imperfect contact model is as follows:

$$\begin{cases} a = a_0 & a \geq 0.1mm \\ a = 0.1 & a < 0.1mm \end{cases}, \tag{9}$$

$$\rho = \eta \rho_{\text{silver}}. \tag{10}$$

The ratio η among different contact fingers has an essential contribution to the current and magnetic field distribution of GIB plug-in connector:

$$\begin{cases} \eta = 1 & a \geq 0.1mm \\ \eta = 0.1/a & 0 < a < 0.1mm \\ \eta = \infty & a = 0mm \end{cases}. \tag{11}$$

B. Electromagnetic field analysis

Electromagnetic field analysis of GIB equipment is conducted by magnetic vector potential **A** and electric scalar potential φ in this paper (**A**-φ method). Maxwell's equations of the quasi-static electromagnetic field in source current region (conductor, V_1), Eddy current region (metal tank, V_2) and non-conductor region (SF_6 and air) can be summarized as follows:

$$\begin{cases} \nabla^2 \mathbf{A} = \mu(\mathbf{J_s} + \mathbf{J_e}) & \text{in } V_1 \\ \nabla^2 \mathbf{A} = \mu \mathbf{J_e} & \text{in } V_2 \end{cases}, \tag{12}$$

$$\nabla^2 \mathbf{A} = 0 \quad \text{in } SF_6 \text{ and Air}, \tag{13}$$

where μ is magnetic permeability, the source current **Js** and the Eddy current $\mathbf{J_e}$ can be shown as:

$$\mathbf{J_s} = -\sigma \nabla \varphi, \ \mathbf{J_e} = -\sigma \frac{\partial \mathbf{A}}{\partial t}, \tag{14}$$

where σ is electrical conductivity.

Boundary conditions on the medium interface of conductor and surrounding gas and the total numerical solution region are described as follows:

$$\left.\begin{array}{l} \mathbf{A_1} = \mathbf{A_2} \\ \mu_1 \nabla \times \mathbf{A_1} \cdot n_{12} = \mu_2 \nabla \times \mathbf{A_2} \cdot n_{12} \\ n \cdot (-j\omega\varepsilon \mathbf{A} - \varepsilon \nabla \varphi) = 0 \end{array}\right\} \text{ on S}, \tag{15}$$

$$\mathbf{A}|_{C1} = 0, \tag{16}$$

where C_1 is the boundary of FEM solution region (air boundary), S is the interface of conductor material and

medium gas, ω is the power angular frequency and ε is the dielectric constant.

V. MAGNETIC FIELD RESULTS

Current and magnetic flux density distributions of GIB equipment under two extreme contact conditions (well assembling and partial loosen contact) under 8000A operation current are investigated by numerical model in this paper. Model parameters are presented in Table 1. The calculated and measured magnetic fluxes around the plug-in connector are compared to each other to verify the validity of numerical calculation model.

Table 1: Geometric parameters of GIB model

Tank material	Aluminum alloy 6063-T6
Bus material	Aluminum alloy 6063-T6
Finger material	Copper alloy T2-Y
Spring material	Beryllium bronze
Finger number	16
Insulator material	Epoxy resin
Tank size	Φ248mm/Φ232mm
Bus size	Φ85mm/Φ65mm
Span	672mm
Field path diameter	107mm

A. Current distributions

Operation currents flow through individual contact finger of GIB plug-in connector under well assembly and partial loosen contact (2 degrees conductor docking angle deviation) are described in Fig. 6. It can be seen from results that the current distributes approximately uniformly among different contact spots under well assembly condition, and maximum current deviation is 189A. However, since seriously contact failure happens, operation currents flow through upper contact fingers (loose contact) decrease to 0 A, whereas current on the bottom contact finger increase up to 1271A.

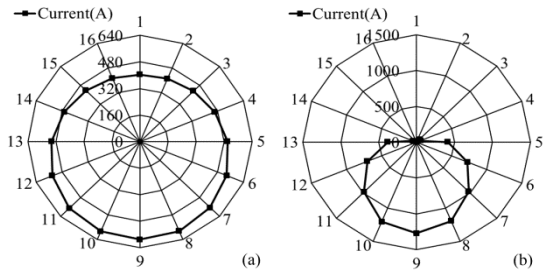

Fig. 6. Current distributions of GIB plug-in connector: (a) well assembly, and (b) conductor docking angle deviation.

B. Magnetic field distributions

The magnetic field distributions of plug-in connector under well assembly (30 mm inserting depth) and partial loosen contact (2 degrees docking deviation) conditions are described in Fig. 7. It can be seen that magnetic flux around each contact finger distributes near uniformly under the well assembly condition. However, when the seriously contact degradation/failure happens, magnetic flux is noticeable distorted and focused around the bottom contact fingers. This is due to the operation current on bottom contact fingers being larger than upper ones with lower contact resistances, exciting larger magnetic field strength round these contact fingers.

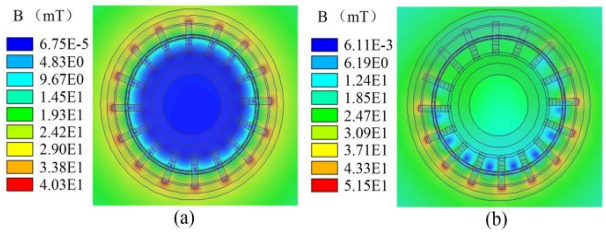

Fig. 7. Magnetic flux density around connector: (a) well assembly, and (b) conductor docking angle deviation.

C. Model verification

Magnetic flux densities around plug-in connector are obtained by both field measurement and numerical modeling. Results are described in Fig. 8. The maximum magnetic flux is averaged for minimize uncontrollable errors during the measuring probes attachment and numerical solution region discretization. Calculated and measured magnetic flux densities around the plug-in connector presents close values since well assembled. Bigger difference can be noticed since contact failure happens with larger field distortions.

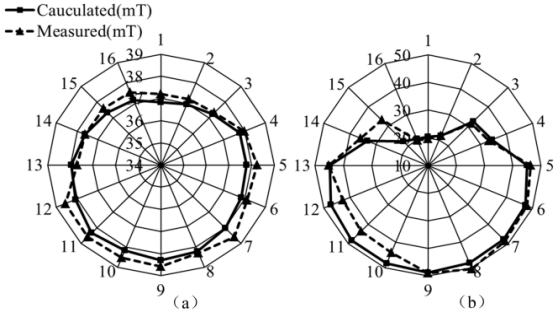

Fig. 8. Magnetic flux around GIB plug-in connector: (a) well assembly, and (b) conductor docking angle deviation.

VI. MAGNETIC FIELD UNDER VARIOUS CONTACT STATUES

The magnetic field distributions around GIB plug-in connector under various contact status are obtained by mechanical-electromagnetic coupling FEM model built in this paper. Operation current is set to 8000A as mentioned before, and the internal contact conditions of GIB plug-connector are constrained by two assembly categories (conductor insert depth and docking angle).

A. Insufficient conductor inserts depth

Figure 9 shows surrounding magnetic field responses under various conductor inserting depths with the same docking angle (0°). Results indicate that the maximum magnetic field strength differs from individual contact fingers of plug-in connector under non-uniform exciting currents. Deviations of magnetic field are not obvious among contact fingers with sufficient conductor insert depth (more than contact failure point). If conductor inserting depth exceeds contact failure point, magnetic field gathers around bottom contact fingers for larger operation currents and lower contact forces. The maximum deviation value of magnetic flux density are increasing with conductor inserting depth decreasing, deviation value is 2mT with the sufficient conductor inserting depth, 5mT at the contact failure point, and 26mT since conductor and connector near separation.

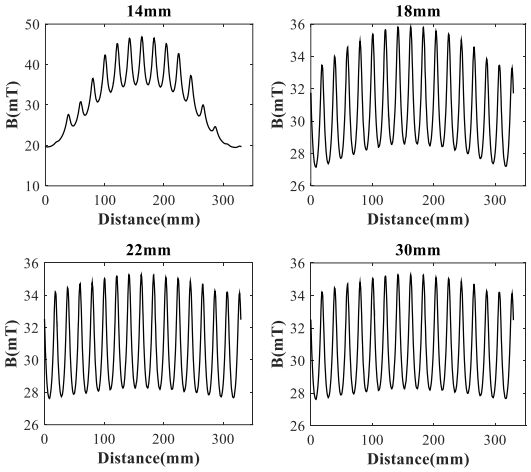

Fig. 9. Magnetic flux strength around plug-in connector under different conductor insert depths.

B. Conductor docking angle deviation (vertical)

Figure 10 shows surrounding magnetic field responses under the various conductor docking angle deviations (vertical direction along the conductor gravity) with the same conductor insert depth (30 mm). Results indicate that the maximum strength of magnetic field differs from vertical contact fingers of plug-in connector under non-uniform exciting currents. Deviations of magnetic field are not obviously among different contact fingers when docking angle less than 2°. If serious conductor docking angular deviation happens, the magnetic field distorts and gathers around contact fingers with lower contact resistances and the larger operation currents. Maximum deviation of magnetic flux density increasing with larger conductor docking angle, and magnetic field deviation value along the conductor gravity (5mT at -0.4° and 30mT at -2°) are larger than those opposite to conductor gravity (1.6mT at +0.4° and 24.5mT at +2°).

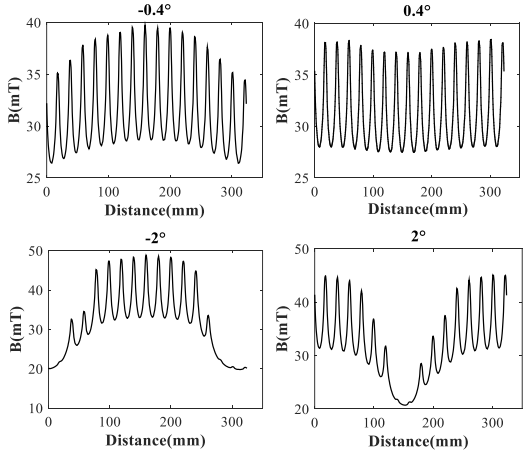

Fig. 10. Magnetic flux around plug-in connector under different vertical conductor docking angles.

C. Conductor docking angle deviation (horizontal)

Figure 11 shows surrounding magnetic field responses under various conductor docking angle deviations (horizontal direction perpendicular to conductor gravity) with the same inserting depth (30 mm). Results indicate that the maximum strength of magnetic field differs from horizontal contact fingers of the plug-in connector under the non-uniform exciting currents. Deviations of magnetic field are not obvious among different contact fingers when docking angle less than 2°. If serious conductor docking angular deviation happens, magnetic field distorts and gathers around left/right side contact fingers with the lower contact resistances and larger currents. Maximum deviation of magnetic flux density increasing with larger conductor docking angles, and the distributions of magnetic field are less influenced by the conductor gravity due to the orthogonal direction. Magnetic field deviation is 5mT at ±0.4°and 30mT at ±2° where conductor is hindered by locating lever.

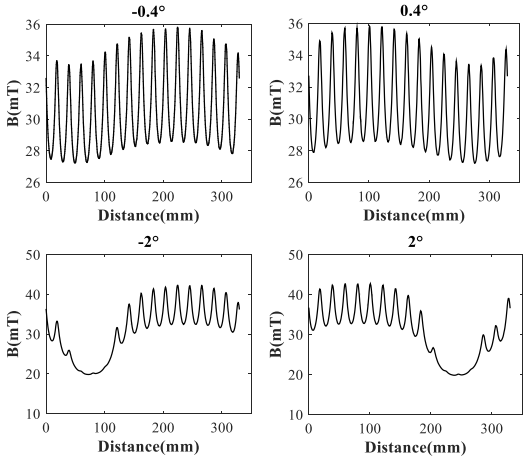

Fig. 11. Magnetic flux around plug-in connector under different horizontal conductor docking angles.

D. Conductor docking angle deviation (arbitrary)

Conductor docking angle deviation θ on arbitrary direction γ can be equivalent by the vector synthesis of horizon direction (x) and vertical direction (y) as follow:

$$\theta\angle\gamma = \theta\cos\gamma + \theta\sin\gamma, \quad (17)$$

where γ is defined by the angle between direction of conductor docking deviation and the horizon axis.

Figure 12 shows surrounding magnetic field responses under the various conductor docking angle deviations (arbitrary direction of 45°) with the same inserting depth (30 mm). Results indicate that the maximum strength of magnetic field around the contact fingers is determined by gravity and the deviation angle of plug-in connector, which could be decomposed into the horizontal and the vertical direction. Deviations of magnetic field are not obvious among different contact fingers when docking angle is less than 2°. If serious conductor docking angular deviation happens, the magnetic field distorts and gathers around the contact fingers with lower contact resistances and larger currents. Maximum deviation of magnetic flux density increasing with larger conductor docking angle, the deviation value is 5mT at ±0.4°docking angle and 25mT at ±2°docking angle where conductor is hindered by locating lever.

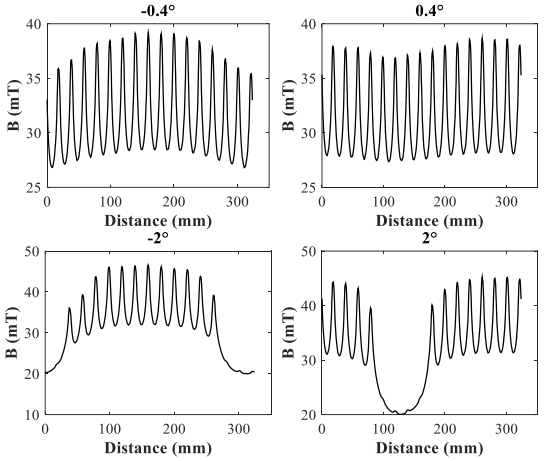

Fig. 12. Magnetic flux around plug-in connector under different 45° conductor docking angles.

VII. CONCLUSION

This work presents a mechanical-electromagnetic coupled FEM model to investigate the magnetic field behaviors of GIB plug-in connector under various assembly conditions and contact failures. The most notable conclusion obtained from this research is that the distribution characteristics of magnetic field around plug-in connector have strong correlation with internal mechanical contact statuses. When assembly conditions between the plug-in connector and conductor change, mechanical contact parameters (forces and radiuses) of different contact fingers deviate, resulting un-uniform distributions of operation current then making magnetic field distorts. The maximum field strength deviation under well assembly condition is about 2mT, and up to 30mT when partial loose contact. According to the analysis results under various contact status, it can be deduced that the surrounding magnetic field can reflect early hidden contact failures of GIB plug-in connector. If significant field deviations occur, equipment is faulty and appropriate action must be undertaken to avoid internal contacts deterioration.

ACKNOWLEDGMENT

This project funded by 60th China Postdoctoral Science Foundation (2016M602352).

REFERENCES

[1] A. Eriksson, K. G. Pettersson, A. Krenicky, et al., "Experience with gas insulated substations in the USA," *IEEE Trans. Power Delivery*, vol. 10, no. 1, pp. 210-218, 1995.

[2] A. E. Emanuel, H. C. Doepken, and P. C. Bolin, "Design and test of a sliding plug-in conductor connector for compressed gas-insulated cables," *IEEE Trans. Power Apparatus and Systems*, vol. 95, no. 2, pp. 570-579, 1976.

[3] Y. Z. Lam, J. W. McBride, C. Maul, J. K Atkinson, "Displacement measurements at a connector contact interface employing a novel thick film sensor," *IEEE Trans. Components and Packaging Technologies*, vol. 31, no. 3, pp. 566-573, 2008.

[4] Y. Mukaiyama, I. Takagi, K. Izumi, T. Sekiguch, A. Kobayashi, et al., "Investigation on abnormal phenomena of contacts using disconnecting switch and detachable bus in 300kV GIS," *IEEE Trans. Power Delivery*, vol. 5, no. 1, pp. 189-195, 1990.

[5] S. Sugiyama, T. Morita, T. Hosokawa, Y. Sekiya, et al., "An investigation of breakdown voltage with small arc current due to poor contact in SF_6 gas," *IEEE Trans. Power Delivery*, vol. 1, no. 7, pp. 332-338, 1992.

[6] M. Runde, O. Lillevik, V. Larsen, et al., "Condition assessment of contacts in gas-insulated substations," *IEEE Trans. Power Delivery*, vol. 19, no. 2, pp. 609-617, 2004.

[7] M. Landry, O. Turcotte, and F. Brikci, "A complete strategy for conducting dynamic contact resistance measurements on HV circuit breakers," *IEEE Trans. Power Delivery*, vol. 23, no. 2, pp. 710-716, 2008.

[8] Y. Ohshita, A. Hashimoto, and Y. Kurosawa, "A diagnostic technique to detect abnormal conditions of contacts measuring vibrations in metal tank of gas insulated switchgear," *IEEE Trans. Power Delivery*, vol. 4, no. 4, pp. 2090-2094, 1989.

[9] N. Okutsu, Y. Takahashi, S. Matsuda, et al., "Pattern recognition of vibrations in metal enclosures of gas insulated equipment and its application," *IEEE*

Trans. Power Apparatus and Systems, vol. PAS-100, no. 6, pp. 2733-2739, 1981.
[10] I. A. Metwally, "Status review on partial discharge measurement techniques in gas-insulated switchgear/lines," *Electric Power Systems Research*, vol. 69, no. 1, pp. 25-36, 2004.
[11] A. J. Reid and M. D. Judd, "Ultra-wide bandwidth measurement of partial discharge current pulses in SF_6," *Journal of Physics D: Applied Physics*, vol. 45, no. 16, pp. 1-10, 2012.
[12] T. M. Lindquist and L. Bertling, "Hazard rate estimation for high-voltage contacts using infrared thermography," 54th *Annual Reliability and Maintainability Symposium*, Las Vegas, USA, pp. 231-237, 2008.
[13] A. Nordstrom and R. Gustafsson, "Magnetic flux density as a probe of the state of electrical contacts," *44th IEEE Holm Conference on Electrical Contacts*, Arlington, USA, pp. 53-56, 1998.
[14] Y. I. Hayashi, "The effect of position of a connector contact failure on electromagnetic near-field around a coaxial cable," *IEICE Trans. Communications*, vol. e92-b, no. 6, pp. 1969-1973, 2009.
[15] H. Fujinami, T. Takuma, and T. Kawamoto, "Development of detection method with a magnetic field sensor for incomplete contact in gas insulated switches and bus connecting parts," *IEEE Trans. Power Delivery*, vol. 10, no. 1, pp. 229-236, 1995.
[16] G. Xiangyu, S. Naiqiu, K. Bing, et al., "Multi-physics calculation and contact degradation mechanism evolution of GIB connector under daily cyclic loading," *IEEE Trans. Magnetics*, vol. 52, no. 3, pp. 1-4, 2016.
[17] R. El Abdi and N. Benjemaa, "Experimental and analytical studies of the connector insertion phase," *IEEE Trans. Components and Packing Technologies*, vol. 31, no. 4, pp. 751-758, 2008.
[18] P. Papadopoulos and R. L. Taylor, "Mixed formulation for the finite element solution of contact problems," *Computer Methods in Applied Mechanics and Engineering*, vol. 94, no. 3, pp. 373-389, 1992.
[19] R Holm, *Electric Contacts, Theory and Applications*. Springer, New York, 1979.
[20] O. Tomohiro, S. Satoshi, and H. Katsuhiro, "Dynamic analysis method of repulsion forces on current-carrying contact using 3-D FEM," *IEEE Trans. Magnetics*, vol. 47, no. 5, pp. 942-945, 2011.

Xiangyu Guan received the B.S. degree of Environmental Science from Xinjiang Normal University, China, in 2010 the M.S and Ph.D. degrees of Power System and Automation from Wuhan University, Hubei, China, in 2015.

He is currently a Lecturer at School of Electrical Engineering Wuhan University. He is Member of ACES and ICS and his research interests mainly focus on electrical contacts, numerical methods of coupling field calculation and condition monitoring of electrical equipment.

Quanyu Shen received the B.S. degree of Electrical Engineering from Hunan University, China, in 2015. He is currently a master candidate in School of Electric Engineering in Wuhan University. His research interests include online monitoring technology and fault diagnosis of electric equipment.

Minghan Zou received the B.S. and M.S. degrees in School of Electrical Engineering Wuhan University, Hubei, China, in 2012 and 2014. He is currently an Engineer in State Grid Nanjing Power Supply Company and his research interest includes electrical equipment monitoring and fault diagnosis technology.

Naiqiu Shu received the M.S. and Ph.D. degrees in Electrical Engineering from Wuhan University. He is currently a Professor in School of Electrical Engineering Wuhan University. His currently research interests mainly focus on sensors technology and its application on condition monitoring of electrical equipment.

Hui Peng received the B.S., M.S. and Ph.D. degrees in Electrical Engineering from Wuhan University. He currently is an Associate Professor in School of Electrical Engineering. His currently research interests mainly focus on condition monitoring of electrical equipment.